communications biology

A Nature Portfolio journal

Article

https://doi.org/10.1038/s42003-026-10205-z

Source-space EEG alpha activity reveals brain age gaps due to neurodegeneration and disparity

Mónica Otero[1], Felipe I. Carriel-Rubilar[2], Hernan Hernandez[3], Jhosmary Cuadros[3], Jorge G. Condado[4], Agustin Sainz-Ballesteros[3], Hernando Santamaria-Garcia[5,6,7], Agustina Legaz[3,8], Agustina Birba[3], Sol Fittipaldi[3,9,10,11], Francisco Lopera[12], John Ochoa-Gómez[12], David Aguillon[12], Alfredis González-Hernández[13], Jasmin Bonilla-Santos[14], Rodrigo A. Gonzalez-Montealegre[15], Görsev G. Yener[16,17,18], Bahar Güntekin[19,20], İlayda Kıyı[21], Tuba Aktürk[22,23], Ebru Yıldırım[24,25], Lütfü Hanoğlu[26], Renato Anghinah[27], Pedro A. Valdes-Sosa[28,29], Ronaldo Garcia-Reyes[28,29], Javier Escudero[30], Susanna Lopez[31], Robert Whelan[9,11], Alberto Fernández[32], Adolfo M. García[8,10,11,33], David Huepe[34], Marcio Soto-Añari[35], Eduar Herrera[36], Daniel Abasolo[37], Nicolás Rubido[38], Ruaridh A. Clark[39], Wael El-Deredy[40], Jesús M. Cortes[4], Mario A. Parra[41], Claudio Babiloni[31,42], Agustin Ibanez[3,8,10,11,19,43,44] ✉ & Pavel Prado[45] ✉

Brain clocks are promising tools for evaluating brain health. However, most current methods rely on structural neuroimaging. Functionally based approaches remain scarce, especially for assessing age-related neurodegenerative diseases. This study examines whether the brain age gap (BAG), the difference between chronological and predicted brain age, reflects neurodegeneration when estimated from electroencephalographic resting-state (rsEEG) α-oscillations, a well-established marker of brain functional aging. It also explores whether α-based brain clocks reflect sociodemographic diversity and structural inequality. The BAG was computed using spectral descriptors of α-activity in the rsEEG source space of 1228 healthy participants, individuals with mild cognitive impairment (MCI), and patients with Alzheimer's disease or behavioral variant frontotemporal dementia, residing in 10 countries with varying levels of structural inequality. BAGs are increased in MCI and dementia groups, particularly in posterior cortical regions. Structural inequality emerges as the strongest predictor of BAG, surpassing cognition, education, and sex. The findings indicate that an α-oscillation-based brain clock provides a sensitive functional marker of brain aging, capable of capturing neurodegenerative processes as well as the impact of social disparities. This scalable, accessible approach to brain health shows promise for translational use and population-wide screening in underserved, resource-limited settings.

AGING comprises the progressive deterioration of physiological functions vital for survival and adaptation[1]. This functional decline varies across physiological systems, suggesting that biological age can be a more reliable indicator of disease susceptibility and mortality than chronological age[2]. In this context, brain clocks, also known as brain age models, compute the discrepancy between an individual's physiological and chronological brain ages (the brain age gap, BAG). Positive BAGs indicate accelerated brain aging, a hallmark or a risk factor of neurodegenerative diseases, inducing cognitive decline to dementia[3–5]. Furthermore, the BAG is influenced by a complex interplay of factors encompassing sociodemographic diversity and socioeconomic disparity[5].

The BAG has traditionally been estimated using structural neuroimaging[3,6–9]. Brain-age models based on functional brain data remain comparatively scarce, especially in the context of neurodegeneration[5,10,11]. Functional information, however, is crucial as disruptions in neural dynamics often precede macroscopic structural damage and behavioral

A full list of affiliations appears at the end of the paper. ✉e-mail: agustin.ibanez@gbhi.org; pavel.prado@uss.cl

alterations during the aging and preclinical phases of neurodegenerative diseases. Recent developments in brain-age modeling, particularly studies using resting-state magneto- and electroencephalography (rsM/EEG), have provided a methodological framework for this purpose[5,12,13]. The rsM/EEG captures brain oscillatory electrical activity under relaxed psychophysiological conditions, typically recorded with eyes closed in an unconstrained, task-free mental state. BAG estimates from these oscillations have been obtained using machine-learning/deep-learning frameworks[13]. In multimodal brain clocks, incorporating rsM/EEG features adds to the information provided by magnetic resonance imaging (MRI), which is primarily driven by 8–30 Hz oscillations[14].

In adults, dominant rsEEG activity is observed at 8–12 Hz in posterior (parietal and occipital) scalp locations[15]. This activity, the α-oscillations, exhibits significant age-related alterations, mainly characterized by frequency slowing[16–18] and reduced spectral power[19,20]. The magnitude of posterior EEG α-activity correlates with cognitive decline in patients with Alzheimer's disease (AD)[21,22], the most prevalent neurodegenerative disease in aging, and distinguishes these patients from healthy control (HC) individuals[23]. Periodic spectral EEG measures are fundamental for capturing individual differences in brain dynamics, outperforming aperiodic EEG components[24]. Likewise, changes in the EEG periodic (oscillatory) activity mostly explain the high-to-low frequency power shift that characterizes AD[25].

In this context, the EuroLAD-EEG Consortium, a platform for dementia research, recently assembled a large database comprising clinical, sociodemographic, and rsEEG data from individuals residing in countries across the Global South and North[26,27]. Initial analyses using this database revealed that variations in rsEEG features, including a reduction in α-oscillation power, were associated with advanced age, poorer cognitive performance, and male sex[24]. Follow-up studies demonstrated that national-level socioeconomic factors, particularly structural inequality, can exert a more significant influence than individual-level characteristics on the complexity, connectivity, and spectral properties of rsEEG, including key descriptors of α-activity[28]. Subsequent investigations on functional cortical networks revealed that structural inequality, environmental pollution, and health disparities significantly increased BAG[5]. Differences in BAG between HC individuals and AD patients, and between males and females, were positively associated with country-levels of structural inequality[5]. Therefore, brain clocks derived from rsEEG α-activity may offer valuable insights into the brain aging trajectories associated with neurodegenerative diseases that induce cognitive decline leading to dementia. This approach is grounded on a brief rsEEG recording, followed by cortical source estimation of well-established quantitative rsEEG descriptors, and the application of artificial intelligence-based algorithms that integrate individual characteristics (e.g., sex and educational attainment as a proxy for cognitive reserve) alongside national-level structural inequality.

This study uses the EuroLAD-EEG database[26] to investigate whether the BAG estimated from source-space rsEEG α-activity progressively increases along a continuum from HC participants to individuals with mild cognitive impairment (MCI) and patients with dementia (AD or behavioral variant frontotemporal dementia, bvFTD). The spectral descriptors of rsEEG α-activity and the EEG source generators most relevant to constructing the brain age model were identified. Then, the contribution of demographics, educational attainment, cognition, income inequality, and clinical diagnosis to the BAG was investigated.

This study introduces a novel, affordable, and straightforward brain clock based on α-oscillations. We used this easy-to-measure EEG metric to examine whether BAG is sensitive to neurodegeneration, sociodemographic diversity, and socioeconomic disparities. The study offers valuable insights into the aging trajectories associated with neurodegenerative diseases[29], highlighting the potential of using rsEEG α-activity to develop tools for screening the risk of cognitive deficits in older adults, a cost-effective strategy especially relevant in resource-limited settings. Using a multicenter design[26], the study explores the generalizability of the results across heterogeneous populations, a critical requirement for robust translational applications.

Results

Increased BAG in neurodegeneration

The rsEEG metrics for brain age modeling were extracted from canonical (fixed) and individualized α-frequency bands. The individualized band was defined using two spectral landmarks: the individual alpha frequency (IAF), identified as the peak frequency with maximum power between 6 and 12 Hz, and the theta–alpha transition frequency (TF), defined as the frequency with minimum power within the 1–6 Hz range[30–32].

The brain age model for EEG α-oscillations yielded adequate goodness of fit ($F = 75.85$, $p < 0.001$, $R^2 = 0.21$, MAE = 6.22, RMSE = 7.78, Cohen$f^2 = 0.13$). The intercept (y_0) of the regression line between chronological age and brain age increased from HC to MCI to bvFTD (Fig. 1A), suggesting that individuals with MCI and bvFTD had greater brain age than age-matched HC participants. The regression line for the AD group had a higher slope (m) and a lower y_0 than that of the HC group (Fig. 1A), indicating that AD patients exhibited elevated brain ages compared to age-matched HC peers, particularly at older chronological ages. The clinical diagnosis exerted a statistically significant effect on BAG ($F_{(3,1257)} = 61.16$, $p < 0.001$, Cohen´s $f = 0.111$) (Fig. 1B). Pairwise multiple comparisons using the Fisher LSD method ($p < 0.05$) revealed that BAG gradually progressed from HC participants to AD patients (Supplementary Tables 1 and 2).

Relevant features for brain clocks of α-oscillations

The power of the canonical α_2 (10.5–12 Hz) and the individual low-α (TF to IAF) and high-α frequency sub-bands (IAF to IAF + 2 Hz)[33] dominated the set of features most relevant for the brain clock of rsEEG α-activity (Fig. 1C). The set of relevant metrics also included the IAF and the TF, the other parameters describing the individual EEG α-frequency band (Supplementary Tables 3–6).

To topographically map the brain clock of α-oscillations, SHapley Additive exPlanations (SHAP)[34] values were computed to quantify the relative importance of each feature within the regression model. Furthermore, anatomically and functionally linked brain compartments were merged into consolidated regions of interest (ROIs) (Supplementary Table 7)[24,28]. For each ROI, the absolute SHAP values of all contributing features were summed and then rescaled to a 0–1 range, yielding a normalized measure of regional importance in brain age prediction. The occipital, parietal, cingulate, and hippocampal brain regions emerged as the most relevant ROIs of the brain clock of α-oscillations in both HC and clinical groups (i.e., MCI, bvFTD, and AD) (Fig. 1D). Other contributing regions were the operculum, orbital cortex, and inferior frontal gyrus (Supplementary Table 8).

Modulating factors of the brain clocks of α-oscillations

The country-level structural inequality was quantified using the Gini coefficient[35] for countries where participants resided during EEG acquisition. Three levels of structural inequality were defined: high, medium, and low (Supplementary Table 9). Country-level structural inequality had a statistically significant effect on the BAG of the HC group ($F_{(2,680)} = 12.52$, $p < 0.001$, Cohen´s $f = 0.185$) (Supplementary Table 10). The pairwise multiple comparison (Fisher LSD Method, $p < 0.05$) showed that the mean BAG of HC individuals increased progressively with increasing levels of structural inequality (Fig. 2A, Supplementary Table 10). Data quality analyses indicate that the results were not affected by the study's multicenter design. Structural inequality was not correlated with the Gini coefficient (Supplementary Fig. 1, Supplementary Table 11), and the mean number of EEG acquisition electrodes did not significantly differ across the levels of structural inequality (Supplementary Fig. 2, Supplementary Table 12). The number of EEG acquisition electrodes did not significantly influence the Overall Data Quality (ODQ) of the EEG estimated in the source space (Supplementary Table 13), with the ODQ being a metric that combines parameters informing about the maximum amplitude, the presence of segments with constant amplitudes, as well as the standard deviation, correlation coefficient, and signal-to-noise ratio of the signals[36]. Neither ODQ,

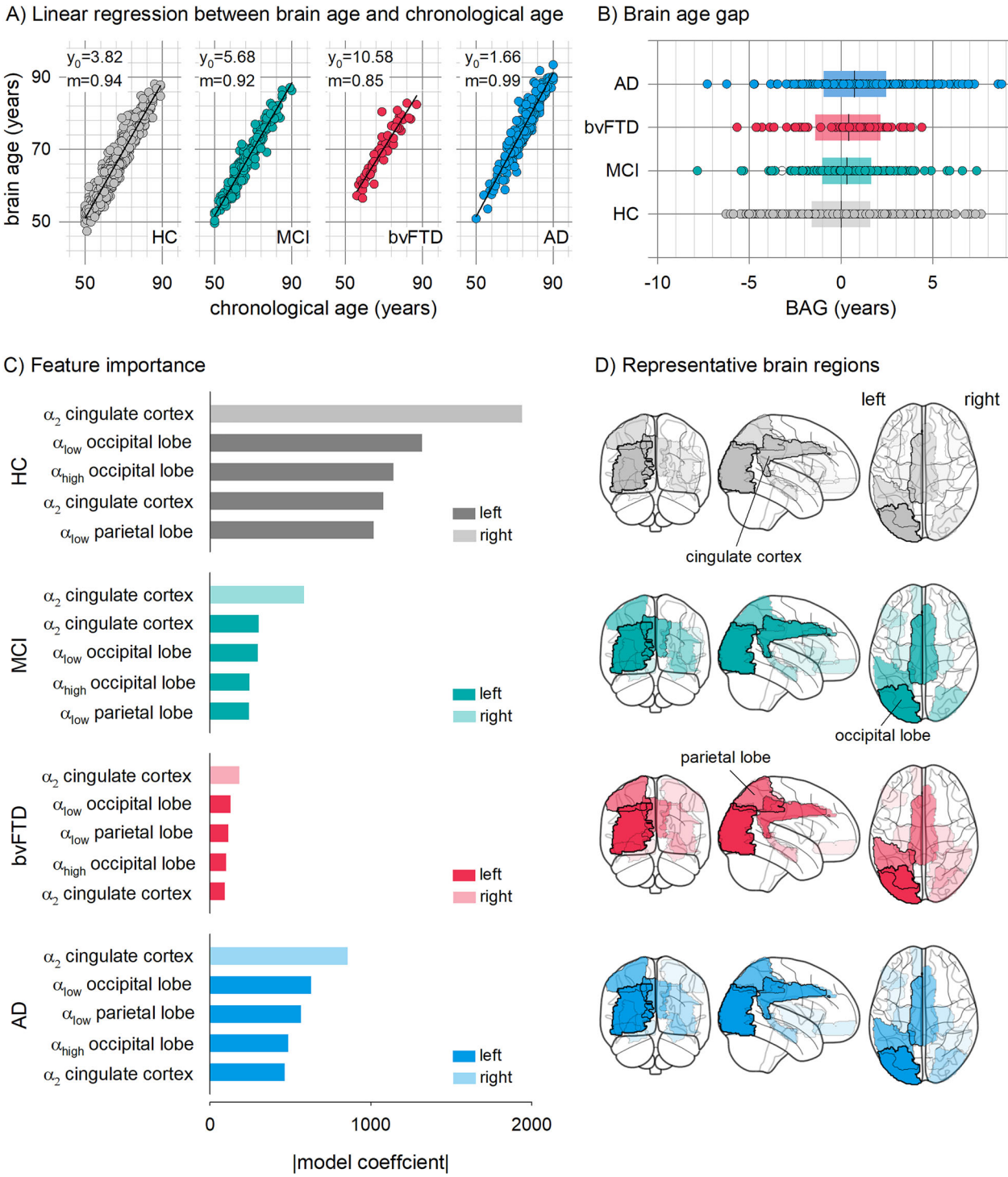

Fig. 1 | Brain age model of source-space EEG α-frequency oscillations. A Linear regression between chronological age and brain age derived from α-oscillations, shown for each participant group. Individual data points (circles) and the corresponding regression line are depicted, with regression parameters detailed for each group. **B** BAG obtained in each group of participants. Circles represent individual values. The horizontal bar represents the median and the 25th/75th percentile of the distribution. **C** Feature importance, ranked by SHAP values. Bar lengths indicate the relative contribution of each feature, with dark and light tones differentiating hemispheric origins. **D** Topographical map of the brain clock of EEG α-frequency oscillations. Representative regions contributing to the brain age model are highlighted in various brain views. Maps in **A** were generated using MapChart (mapchart.net) and are used under the CC BY-SA 4.0 license. The icons representing filtering, resampling, and artifact correction in **C** were obtained from iStockphoto.com through a paid subscription. The human silhouette used in the acquisition schematic of **C** was obtained from Shutterstock.com through a paid subscription. The source-localization schematic in **C** was created by the authors to match the silhouette in the acquisition panel, and the brain graphic in the source-localization panel was adapted from Servier Medical Art (SMART) under the CC BY 4.0 license. Some of these licensed third-party elements were also reused in the Graphical Abstract, and the same credit and licensing information applies to those elements.

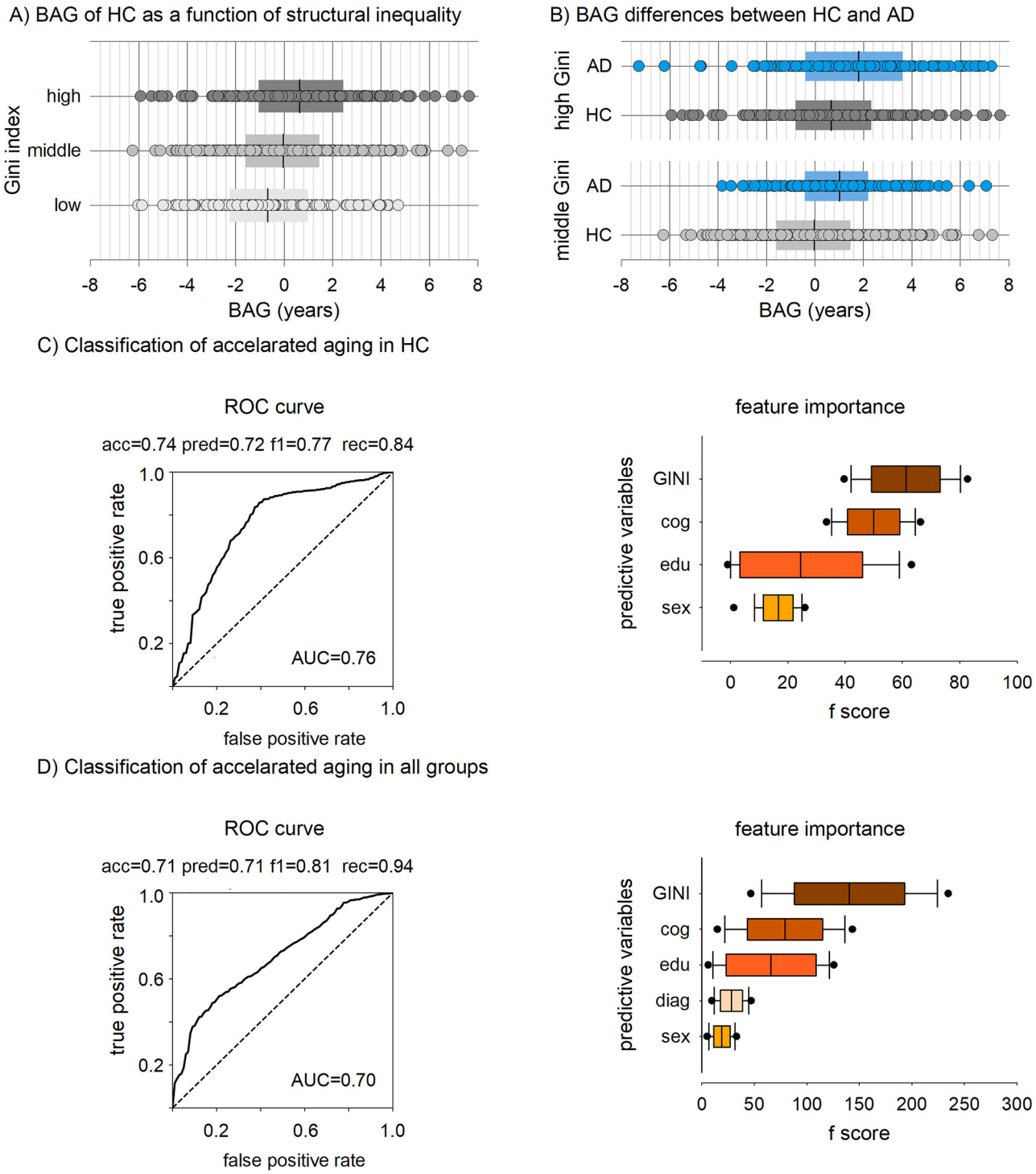

Fig. 2 | Group-level statistics of the brain age gap (BAG) estimated from source-space rsEEG α-activity and classification of accelerated vs. delayed brain aging. **A** Mean BAG comparison of HC across groups of countries with diverse structural inequality. **B** Mean BAG variations as a function of the group of participants (diagnosis) and structural inequality. The analysis only considered two categories of country-level structural inequality and two groups of participants (HC and AD). In **A** and **B**, the circles represent individual values, and the horizontal bar represents the median and the 25th/75th percentile of the distribution. **C** Classification of accelerated vs. delayed brain aging in HC. **D** Classification of accelerated vs. delayed brain aging in the entire sample. In **C** and **D**, the panels from left to right illustrate the ROC curve, the confusion matrix, and the relative importance of the predictive variables in the classification. Measures of the classification performance are outlined. acc: accuracy, pred: precision, rec: recall. The box plots represent the mean (solid vertical line) and the 25th/75th percentile of the distribution, with points representing the 5th/95th percentile of the distribution.

the number of participants, nor the number of channels predicted Gini (Supplementary Table 14).

When the group-level analysis included both HC participants and AD patients, and the categories of country-level structural inequality were restricted to middle and high (Fig. 2B), both structural inequality ($F_{(1,823)} = 15.71$, $p < 0.001$, Cohen´s $f = 0.209$) and clinical diagnosis ($F_{(1,823)} = 36.05$, $p < 0.001$, Cohen´s $f = 0.138$) showed statistically significant effects on BAG (Supplementary Table 10). The interaction between

these factors ($F_{(1,823)} = 0.08$, $p = 0.769$, Cohen´s $f = 0.010$) showed no statistical effect. A higher BAG was linked to living in countries with increased structural inequality (Fisher LSD method, $p < 0.05$). In countries with similar Gini coefficients, the mean BAG of the AD group was statistically significantly higher than that of the HC participants (Fig. 2B, Supplementary Table 15).

Furthermore, country-level structural inequality, cognitive status (assessed using the raw total score from the Mini-Mental State Examination, MMSE)[37], educational attainment, and sex contributed to distinguishing between HC individuals with increased vs. delayed brain aging, defined by BAG values above and below the median of the BAG distribution (Fig. 2C). The classification yielded moderate performance (AUC of ROC curve: 0.76, accuracy: 0.74, precision: 0.72, F1-score: 0.77, recall: 0.84). The country-level structural inequality was the most influential predictor of BAG, followed by the cognitive status, educational attainment and sex (Fig. 2C). Expanding the analysis to include both HC and clinical groups and incorporating clinical diagnosis as an additional predictive variable also resulted in an adequate classification of individuals with increased vs. delayed brain aging (AUC of the ROC curve: 0.70, accuracy: 0.71, precision: 0.71, F1-score: 0.81, recall: 0.94) (Fig. 2D). Structural inequality remained the most influential predictor, followed by cognitive status, educational attainment, clinical diagnosis, and sex (Fig. 2D).

Discussion

We investigated brain clocks of EEG α-activity in a cohort of 1228 participants (50–90 years) of both sexes with different clinical statuses (i.e., HC, MCI, bvFTD, and AD) and varying cognitive reserve, as reflected by their educational attainment. They were enrolled in 10 countries with different structural inequalities. Results showed that the BAG was significantly related to rsEEG α-activity estimated in the occipital, parietal, cingulate, frontal, and hippocampal brain regions. BAG was also effectively related to diversity and disparity. At the group level, increased BAG was associated with higher country-level structural inequality and neurodegeneration. Furthermore, country-level structural inequality emerged as the most influential predictor of BAG at the individual level, surpassing cognitive status, educational attainment, and clinical diagnosis.

This study demonstrates that BAG, estimated using an easily interpretable and clinically accessible EEG signature of brain function, is sensitive to neurodegeneration, individual diversity, and socioeconomic disparities. The model offers insights into age-related changes through well-described oscillatory dynamics, thereby complementing traditional brain age models based on T1-weighted morphometry or diffusion-based connectivity estimates. The α-oscillations measures are well-recognized indicators of aging and cognitive decline. However, this is the first time these measures have been used to develop sensitive brain clocks. The study's multicenter design enhances the generalizability of the findings across diverse populations, underscoring the importance of socioeconomic variables in assessing brain aging.

Group differences in BAG

The brain clock of α-oscillations showed adequate goodness of fit (Fig. 1), with an MAE within the range reported in previous EEG-based brain age models (5–12 years)[5,13,38,39]. Although higher than the MAE typically observed in MRI-based approaches, this is expected, as functional brain clocks capture dynamic neural processes that are not accessible through structural imaging[4]. Notably, while tightly fitting brain-age models minimize error, they often yield predictions that provide limited information beyond chronological age[6]. Moderate-fitting models, such as the α-frequency brain clock, can exhibit greater sensitivity to neurodegeneration and sociodemographic influences. Furthermore, the MAE reported in this study is consistent with single-site EEG studies[13] despite the added variability of a multicenter design. Multicentric studies enhance the generalizability of results[4] and enable assessment of sociodemographic influences on brain age, thereby providing greater translational value for clinical and population-based applications.

The linear relationship between the brain age estimated from α-frequency oscillations in the EEG-source space (Fig. 1A) and chronological age supports previous studies demonstrating linear associations between age in older adults and the magnitude of those oscillations[19], a result with potential clinical applications for population-based aging screening. Furthermore, the findings indicate that alpha-band EEG activity reflects meaningful deviations from normative brain aging trajectories among individuals with MCI and dementia, highlighting the role of clinical status in shaping these trajectories. This result aligns with and complements previous studies using other neuroimaging approaches[5,40,41]. However, the mean BAG differences among groups were modest, with BAG distributions showing substantial overlap (Fig. 2B). This is not unexpected, as the present brain age model was restricted to a single EEG frequency band. Greater discriminative power can be anticipated from integrative approaches that combine a larger number of spectral descriptors with complementary EEG domains, including complexity and connectivity measures. The variability observed in our BAGs (2.1–2.8 years, Supplementary Table 1) aligns with previous reports from both EEG- and MRI-based studies[5,13], where variability depends on the modality and analytic pipeline employed[4,38,42]. The effect sizes obtained in this study further indicate that factors beyond clinical diagnosis contribute substantially to the explained variance of BAG. This interpretation is supported by our classification analyses, which demonstrated that structural disparity, cognition, and education exert stronger modulatory influences on BAG than clinical diagnosis of brain health (Fig. 2D).

The increased BAG of MCI individuals and patients with dementia can, in part, be attributed to the atrophy of the posterior cortical generators of rsEEG α-frequency oscillations. Abnormalities in those oscillations have been linked to reduced cortical gray matter volume in individuals with MCI and patients with AD[43]. Increased BAG can also reflect disrupted cholinergic activity in the basal forebrain and its connections to the thalamus and posterior cerebral cortex that regulate cortical arousal and vigilance, a hallmark of neurodegenerative conditions such as AD[32,44,45]. This dysfunction may lead to altered oscillatory dynamics within thalamic and cortical networks that generate the brain α-rhythm[45,46], which critically depend on the integrity of the forebrain cholinergic pathways and their cortical targets[47].

The rsEEG α-predictors of BAG

EEG metrics derived from individual α-frequency bands were relevant to brain age estimates (Fig. 1C, Supplementary Tables 3–6). This is consistent with previous research showing that power descriptors of individual EEG α-activity enable the accurate classification of HC and AD individuals[32,48]. Compared with the canonical approach, individualized α-frequency bands more sensitively capture age-related slowing of rsEEG rhythms and the decline in IAF observed in AD and related neurodegenerative disorders[48], effects driven primarily by changes in periodic oscillatory activity rather than by non-oscillatory (aperiodic) components[25].

Overall, the findings underscore the core role of the low α-frequency sub-band in BAG estimations (Fig. 1C, Supplementary Tables 3–6). The power of this EEG frequency sub-band has been considered a neural correlate of the participant's global attentional readiness and aging[19,49]. Its reduction may reflect the desynchronization of dominant posterior rsEEG rhythms, a phenomenon associated with neurodegenerative processes, including the progression of AD[50].

Topographic representation of the α -brain clock

Key regions governing the brain clock for EEG α-activity, including the occipital, parietal, and cingulate cortices, exhibit decreased and disrupted α-oscillations in aging and neurodegeneration[19,51]. In AD patients, the magnitude of α-oscillations has been associated with occipital cortical volume[52,53]. Altered EEG α-power has also been linked to hippocampal and parietal atrophy[54,55], both of which are key brain regions for the brain clock of α-oscillations (Fig. 1D). These results align with previous findings indicating a systematic decline in EEG α-power estimated in the limbic and parietal brain regions as individuals age[19], a pattern pronounced in AD patients[51].

Moreover, these findings are consistent with computational modeling studies suggesting that EEG α-power and the IAF are contingent upon the number and synchrony of neurons within the cortical generators of α-oscillations[56].

Although the cingulate cortex is cytoarchitectonically and functionally heterogeneous, it exhibits significant atrophy in Alzheimer's disease when considered as a whole, highlighting its vulnerability to neurodegeneration[57]. The volume of posterior cingulate cortex and other default mode network (DMN) regions positively correlates with rsEEG α-source activity and global cognitive status in older individuals[58]. Compared with HC participants, AD patients exhibit reduced DMN gray matter volume, diminished rsEEG α-source activity in those regions, and lower global cognitive status[58]. Similarly, parietal cortical areas integral to the DMN, including the postcentral and supramarginal gyri, exhibit severe atrophy in patients with bvFTD[59,60].

Demographic diversity and structural inequality are reflected in the α-brain clock

The BAG estimated from rsEEG α-activity progressively increased with rising levels of structural inequality (Fig. 2A, B). This finding complements studies suggesting that country-level structural inequality modulates EEG source-space dynamics[28] and that differences in BAG between HC individuals and AD patients widen as country-level structural inequality increases[5]. Higher country-level structural inequality is associated with reduced source-space rsEEG α-power, particularly in the cingulate cortex and the parietal lobe[28], two of the brain regions with the highest preponderance in the brain clock of rsEEG α-activity (Fig. 1D). The rsEEG α-activity estimated in regions critical for mapping brain aging trajectories (occipital and parietal lobes) (Fig. 1D) is also modulated by sex, educational attainment as a proxy of cognitive reserve, and cognitive status[24]. Notably, EEG spectral metrics most affected by cognitive status (power in the α_2 and low-α EEG frequency bands)[24] were also ranked among the most significant contributors to the brain age model (Fig. 1C).

The heterogeneous influence of diversity and disparity on the BAG of HC participants (Fig. 2C) emphasizes the profound impact of country-level structural inequality on brain dynamics, which can exceed the significance of general cognitive status and educational attainment[28,61]. The relatively lower influence of sex on brain age compared with other variables (Fig. 2C) aligns with findings from other multifactorial analyses conducted across diverse populations[24,28].

While BAG varied significantly across participant groups (Fig. 1B), clinical diagnosis was not the primary determinant of BAG outcomes (Fig. 2D). Instead, its effect was surpassed by the influence of country-level structural inequality, general cognitive status, and education attainment (Fig. 2D). Although challenging, this result does not represent an isolated observation since previous studies illustrate that clinical diagnosis can be outweighed by the cognitive status and educational attainment even when brain health is evaluated behaviorally[62]. This emphasizes the complex interplay between physiological and environmental factors that underlie brain aging trajectories and the relevance of adopting multidimensional approaches to assess brain health[63].

Methodological remarks

The following methodological limitations should be considered when interpreting the results. The study is characterized by an unbalanced sample, with the recruitment of participants with neurodegenerative diseases confined to specific countries with middle and higher structural inequality. Future research must strengthen cross-country and cross-regional analyses by employing representative cohorts that span broader geographic and demographic contexts. Furthermore, longitudinal studies are imperative for elucidating brain aging trajectories and disease progression[64]. Notably, future studies should incorporate the age of disease onset and disease duration at the time of EEG recording as predictors of BAG, considering that different cognitive impairments are associated with early- and late-onset AD[65]. Similarly, incorporating individual-level demographics and socioeconomic indicators, such as gender identity, ethnicity, household income, and quality of education, will enhance the understanding of social diversity and provide a more comprehensive perspective on disparity beyond country-level indices. Finally, expanding the set of cognitive assessment tools beyond the MMNE to include cognitive social variables such as empathy and compassion will help to capture the full spectrum of mental abilities.

EEG acquisition and processing challenges that may affect model outcomes include the use of diverse electrode configurations, the use of an average brain template for EEG source space estimation, and the choice of ROI definitions. EEG scalp topographies derived from different electrode layouts were integrated using a head mesh model of 1082 electrodes[66,67]. This is an alternative to spatial harmonization procedures implemented in other multicenter studies, which are based on assigning equivalent electrodes according to distances[68,69]. In our study, the number of EEG electrodes was not correlated with the Gini coefficient (Supplementary Fig. 1, Supplementary Table 11) or with the mean Gini index of each of the three country-level structural inequality categories used in BAG comparisons (Supplementary Fig. 2, Supplementary Table 12). As in previous studies using this dataset[24,28], the number of channels used for EEG acquisition did not predict the signal quality in the EEG source space (Supplementary Table 13). This is in accordance with analyses conducted in the group of HC, which demonstrate that neither the ODQ, the number of HC individuals per recruitment center, nor the number of EEG acquisition channels predicted the country-level structural inequality (Gini coefficient) when this outcome was assessed using logistic regressions[28] (Supplementary Table 14). Future research should leverage high-density electrode arrays and individual MRI data to increase the resolution and robustness of EEG source-space estimates, refining the interpretation of individual differences across diverse populations and advancing our understanding of brain health.

Methods

Participants

The dataset used in this study[26] comprises rsEEG recordings from 1319 individuals residing in Argentina, Brazil, Chile, Colombia, Cuba, Greece, Italy, Ireland, Turkey, and the United Kingdom (Fig. 3A). A portion of this dataset has been used in studies on dementia[70–75] and is publicly available[27]. The Institutional Ethics Committees of each participating center approved the collection and use of de-identified data, with participants providing informed consent in accordance with the Declaration of Helsinki. All ethical regulations relevant to human research participants were followed.

Participants were categorized as HC, MCI, bvFTD, or AD, and grouped by the Gini coefficient of their respective nations at the time of data collection[5,28,61]. This coefficient quantifies deviations in income distributions within an economy from perfect equality[35] and ranges from 0 to 100, where 0 indicates perfect country-level equality, and 100 represents complete country-level inequality[76]. Three levels of structural inequality were defined: high, medium, and low (Fig. 3B, Supplementary Table 9). This classification, along with information on age, educational attainment, cognitive status, and clinical diagnosis of the participants (Fig. 3C, Table 1), was incorporated into subsequent analyses.

The cognitive status was assessed using the raw total score from the Mini-Mental State Examination (MMSE)[37], a valuable instrument for general cognitive assessment in clinical and research contexts[77]. The MMSE scores range from 0 to 30, with scores ≤ 24 indicative of abnormal cognitive function. Participants with MCI met the Petersen criteria, with MMSE scores below the cut-off threshold 24[78]. Clinical diagnosis of AD was based on the current criteria of the National Institute of Neurological Disorders and Stroke–Alzheimer's Disease and Related Disorders (NINCDS-ADRDA) working group for probable AD[79]. Likewise, patients with bvFTD fulfilled the revised criteria for probable bvFTD[80].

EEG recording, processing, and normalization

The rsEEG was recorded using scalp electrodes under eyes-closed and general psychophysical relaxation conditions, with participants seated comfortably in an armchair. Electrooculographic activity was also recorded

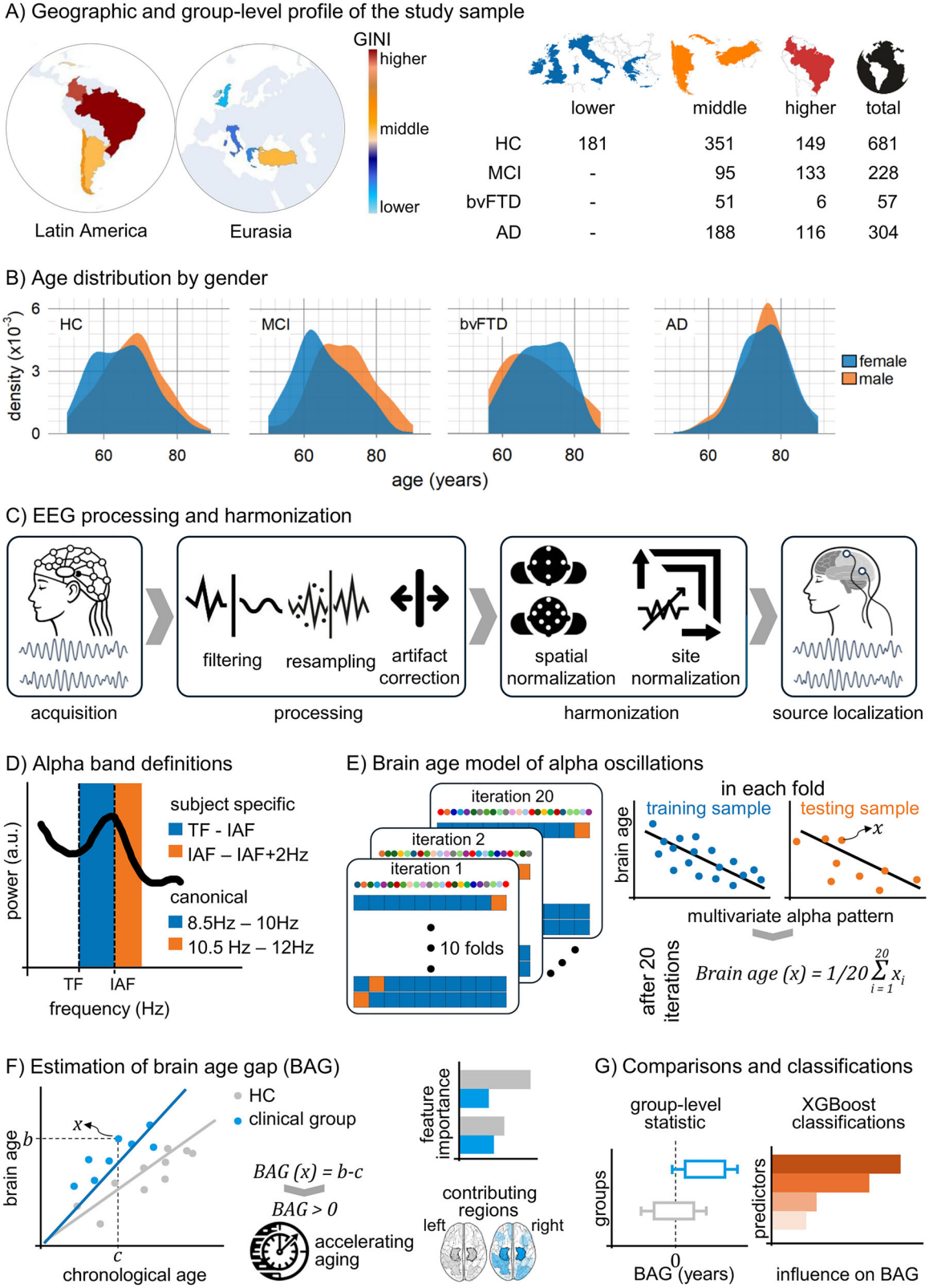

to control eye movements and blinking. Antialiasing, analog filtering, and frequency sampling were performed before digital storage. The EEG acquisition setting used at each recruitment center is reported in Supplementary Table 16.

The rsEEG was processed using an automatic pipeline that included protocols to mitigate cross-site methodological variations[81–83], which has been adopted in studies on brain age[5], social diversity[24], country-level socioeconomic disparity[28], and dementia[5,73,75]. The EEG was filtered between 0.5 and 40 Hz, re-sampled to 512 Hz, and re-referenced using the reference electrode standardization technique[84] (Fig. 3C). Blinking, ocular artifacts, and myogenic activity were corrected using ICLabel (a tool for the classification of EEG-independent components into signals and different

Fig. 3 | Methodological framework for brain age gap (BAG) estimation using EEG α-oscillations. A Geographic and group-level characterization of the study sample. Countries were grouped into lower, middle, and higher structural inequality categories based on the GINI coefficient, with distinct colors representing each group. The participant numbers per group are indicated. **B** Age distribution stratified by group and sex. **C** Key processing and harmonization steps for the estimation of α-oscillations in the EEG source space. **D** Definitions of the EEG α-band adopted in the study. The bandwidth limits are presented in each case. **E** Workflow for constructing the brain age model of α-oscillations, including data splitting and repetition procedures used to obtain brain age estimates for every participant. **F** BAG computation. The panel illustrates group-level brain aging, defines accelerated aging, and presents an analysis of feature importance alongside a topographical representation of the brain clock for α -oscillations. **G** Group-level statistics and classification of BAG. Group-level variations in BAG were investigated as a function of the country-level structural inequality and the participant group. Accelerated vs. slowed brain aging was classified using predictive variables such as country- and individual-level measures of diversity and disparity, as well as diagnosis.

Table 1 | Details of the study sample

Group	Relative GINI	Country	*N*	F:M ratio	Age	Years of education	Cognition
HC	Low	Ireland	85	41:44	67.6 ± 5.5	15.2 ± 4.0	29.0 ± 1.0
		UK	50	25:25	68.7 ± 7.8	16.1 ± 6.0	–
		Greece	24	10:14	68.8 ± 5.3	–	30.0 ± 0.0
		Italy	22	13:9	61.7 ± 7.9	15.3 ± 5.0	–
	Middle	Cuba	9	7:2	58.3 ± 4.4	12.1 ± 1.8	29.8 ± 0.5
		Argentina	40	29:11	66.5 ± 8.3	17.7 ± 2.3	28.9 ± 0.8
		Turkey	252	152:100	66.1 ± 8.2	11.0 ± 5.3	29.0 ± 1.2
		Chile	50	35:15	70.1 ± 7.1	14.8 ± 4.3	28.8 ± 1.4
	High	Colombia	77	60:17	59.5 ± 6.4	13.7 ± 5.1	27.9 ± 1.7
		Brazil	72	42:30	67.8 ± 10.0	12.1 ± 3.6	27.8 ± 1.5
MCI	Middle	Turkey	95	45:40	73.2 ± 6.5	8.9 ± 4.4	25.0 ± 3.6
	High	Colombia	133	111:22	62.5 ± 6.2	8.1 ± 5.4	27.0 ± 1.7
bvFTD	Middle	Argentina	33	13:20	69.5 ± 9.1	14.8 ± 4.6	26.9 ± 3.8
		Chile	18	12:6	70.7 ± 5.9	14.6 ± 3.7	23.1 ± 4.7
	High	Colombia	6	2:4	66.5 ± 5.8	7.8 ± 6.7	21.8 ± 4.7
AD	Middle	Argentina	32	19:13	73.8 ± 7.5	9.9 ± 5.0	23.7 ± 3.3
		Turkey	96	62:34	74.2 ± 5.1	8.8 ± 4.4	19.9 ± 4.8
		Chile	60	26:34	71.2 ± 7.0	12.4 ± 4.9	21.5 ± 4.0
	High	Colombia	44	30:14	72.7 ± 5.6	13.5 ± 3.8	21.3 ± 3.4
		Brazil	72	49:23	80.7 ± 6.6	10.1 ± 4.3	21.0 ± 4.5

HC healthy controls, *MCI* mild cognitive impairment, *bvFTD* behavioral variant frontotemporal dementia, *AD* Alzheimer's disease

categories of noise)[85] and EyeCatch (a tool for identifying eye-related scalp EEG maps)[86]. Noisy channels were replaced using weighted spherical interpolations[66]. *Z*-score transformations of the EEG time series were computed independently for each recruitment center to reduce inter-site variability[70,73]. The artifact-free EEG activity derived from the electrode montage used at each recruitment center was interpolated to produce datasets with a 128-radial electrode layout, using a mesh-head model of 1082 virtual electrodes, as implemented in the EEGLAB headplot function[87]. This approach has been employed as a spatial normalization method in studies examining between-subject and between-session variances across EEG acquisition[87], and has been implemented in previous multicenter EEG studies[5,24,28]. Transforming low-density electrode configurations into high-density montages implies generating virtual channels that carry redundant information from the original signals. While this transformation does not imply a gain of information, it reduces the dependence of EEG source estimation on the number of electrodes when applying inverse solution models, whose spatial resolution is inherently constrained under low-density electrode setups.

EEG source estimation

EEG brain sources (Fig. 1C) were estimated using the standardized low-resolution electromagnetic tomography (sLORETA) method implemented in the LORETA KEY software[88,89]. Standardized current density maps were computed within the 6242 voxels (5 × 5 × 5 mm each) of the sLORETA brain model, for each of the 153,600 voltage distributions corresponding to the first five minutes of artifact-free rsEEG. The sLORETA head model consisted of three concentric spheres, and a signal-to-noise ratio of 1 was used as a regularization parameter of the sLORETA transformation matrix. A brain segmentation of 82 compartments was implemented using the Automated Anatomical Labeling (AAL) atlas[90]. The inverse solution for each scalp voltage distribution yielded the estimated current-density time series across all voxels of the sLORETA head model. The time series for voxels corresponding to the same AAL brain region were averaged to yield the mean brain source time series for that specific AAL region[71,72].

EEG parameters

The normalized power spectral density (nPSD) for each AAL brain region was calculated using Welch's method, employing a 4-s Hanning window with 50% overlap, resulting in a spectral resolution of 0.25 Hz[91,92]. The canonical α-frequency sub-bands were alpha1 (α1), ranging from 8.5 to 10 Hz, and alpha2 (α2), spanning 10.5–12.0 Hz[33]. The individual α-frequency sub-bands were defined as low-α (TF to IAF) and high-α (IAF to IAF + 2 Hz)[33] (Fig. 1D). Using the canonical definition of α-frequency sub-bands ensured cross-study comparability in brain aging. At the same time, the individualized approach accounted for the typically lower IAF observed in AD patients compared with HC individuals[30,31].

The relative power density (RPD, the mean nPSD) was calculated for each canonical and individual α-frequency sub-band. Additionally, the equivalent percent power (EPP) of each α-frequency sub-band, representing the proportion of nPSD within the sub-band relative to the total nPSD, was computed[33,93,94]. These parameters (RDP and EPP), IAF, and TF were used for BAG assessments.

Reduction of the EEG analytical space

Resting state α-activity can be detected in most regions of the human brain, although it typically co-exists with oscillatory activity in other E/MEG frequency bands[95]. To streamline the analysis of α-activity, anatomically and functionally linked AAL compartments were merged into consolidated regions of interest (ROIs), as described in previous studies using the EuroLAD-EEG dataset[24,28]. For example, neighboring brain regions with established functional coupling, such as the hippocampus, parahippocampal area, and amygdala, were grouped, as were areas within a given cerebral lobe, such as the calcarine fissure and surrounding cortex, the cuneus, the lingual gyrus, and the superior, middle, and inferior occipital gyri. This procedure resulted in ten cohesive ROIs (Supplementary Table 6), allowing reliable detection of both the IAF and the TF within each ROI. The same ROI selection has been applied in previous studies investigating associations among the EEG spectrum, sociodemographic diversity, and country-level structural inequalities[24,28]. Focusing on ROIs that encompass structurally and functionally interconnected areas accounts for the inherently low spatial resolution of EEG inverse solution methods, thereby enhancing data interpretation and facilitating the identification of meaningful patterns in brain activity[24,28]. This reduction of the EEG analytical space mitigates the effects of the EEG electrode configuration, given the increased variance that can arise from using spatially harmonized EEG signals from both low- and high-density electrode configurations. Comparable dimensionality-reduction strategies have been applied in other dementia studies investigating brain oscillations in the EEG source space[52,96].

BAG estimation

A linear regression model was constructed to estimate brain age from EEG features using Elastic Net[97]. This regularization technique controls model complexity by balancing feature selection and coefficient shrinkage. Penalties in the model promote sparsity by setting some coefficients to zero, enabling feature selection and shrinking correlated coefficients toward similar values, thereby mitigating multicollinearity and overfitting. Elastic Net is advantageous for assessing high-dimensional datasets with correlated predictors[98], thereby ensuring robustness and interpretability in brain age prediction.

Brain ages were computed using bagging, an ensemble learning technique that enhances predictive accuracy and reduces variance by training multiple models on bootstrapped subsets of the data and averaging their outputs[99]. Bagging is an ensemble learning method that generates multiple models by training on different subsets of the data and then averaging the predictions. In this study, 20 brain age estimates were obtained for each participant and subsequently averaged to enhance reliability. For each data subset, the HC sample was split into 90% and 10% for training and testing, respectively[100]. The model was trained using 10-fold cross-validation (Fig. 3E). Furthermore, the regression model obtained during each cross-validation iteration was used to estimate the brain age of one-tenth of the individuals in each clinical group. This process was repeated 20 times, with the data randomly shuffled in each iteration[100]. Consequently, 20 brain age estimates were generated for each participant, with the mean serving as the final brain age prediction (Fig. 3E). The BAG was calculated as the difference between each individual's actual chronological age and the mean brain age prediction. A positive BAG (BAG > 0) indicated that the brain's functional age appeared older than expected for the individual's chronological age. Conversely, a negative BAG (BAG < 0) indicated that the brain's functional attributes resembled those of younger peers (Fig. 3F).

A bias systematically exhibited by brain age models is the overestimation and underestimation of brain age in younger and older individuals, respectively, such that brain age is more accurately predicted for participants with a chronological age closer to the mean age of the training dataset[101]. This regression-toward-the-mean bias was adjusted in each cross-validation fold by linearly regressing the chronological age of the training set on the BAG estimates and using the regression residuals to correct the BAG estimates. Subsequently, the regression coefficients were used to adjust the BAG for individuals comprising the test set[5,29].

For each cross-validation fold, we computed the coefficient of determination (R^2), the mean absolute error (MAE), the mean squared error (MSE), Fisher's F, and the model's significance. These metrics were used to evaluate the model's performance. Furthermore, SHapley Additive exPlanations (SHAP) values[34] were computed to evaluate the relative importance of each feature in the regression models (Fig. 3F).

BAG classifications

An XGBoost classifier was used to distinguish HC participants with low and high BAG, using country-level structural inequality (measured by the Gini coefficient), demographic factors (sex and educational attainment), and cognitive status (MMSE score) as predictive variables. The BAG was binarized using the median (−0.09) rather than zero to ensure a balanced class distribution. A second XGBoost classifier was used to predict low versus high BAG across the entire sample as a function of the clinical diagnosis (i.e., HC, MCI, bvFTD, AD), demographic factors (sex and educational attainment), and cognitive status. For model training and evaluation, the data was split into 80% for training and 20% for testing. A k-fold ($k = 10$) cross-validation was used in the training phase. Performance classification metrics were reported, including accuracy, precision, and recall.

Statistics and reproducibility

The study sample size (1319 participants) exceeded the minimum threshold required to detect a small effect size (Cohen$f^2 = 0.04$) in multiple linear regression analyses (F test, fixed model) and a medium effect size (Cohen's f=0.15) in fixed-effects ANOVA (F test, main effects, and interactions), ensuring a statistical power of 0.95[102].

A Welch´s ANOVA ($p < 0.05$) was performed to compare the mean BAG across groups and to examine variations in the BAG of HC as a function of structural inequality (Fig.3A, Table 1). This parametric test was chosen due to its suitability for cases where the study has a large sample size, but the assumption of homoscedasticity is not met[103]. Furthermore, a two-way ANOVA ($p < 0.05$) was conducted to analyze variations in BAG as a function of the structural inequality of the country of residence and participants' clinical diagnosis. The factor "structural inequality" included two levels: middle and high Gini, while the factor "group" comprised HC and AD. Unfortunately, restricting the ANOVA factors to two levels was necessary due to the absence of a representative sample of AD patients from countries classified in the lower GINI group and the limited geographical distribution of MCI and bvFTD patients (Table 1). For example, the MCI sample from medium-Gini-level countries comprised only Turkish participants, while the high-Gini-level bvFTD sample included only Colombian participants. The Fisher LSD test ($p < 0.05$) was the post hoc test for multiple comparisons in all statistical analyses.

To analyze the effect of possible confounders, we assessed whether the number of electrodes across sites influenced the results by testing associations between the number of EEG electrodes and country-level structural inequality. Additionally, consistent with our previous studies[24,61], the ODQ index[36] of the EEG signals estimated in source space was used to control for potential confounds related to electrode number, sample size, and structural inequality. The ODQ quantifies the proportion of high-quality epochs in a recording by integrating signal-quality parameters such as maximum amplitude, standard deviation, correlation coefficient, and signal-to-noise ratio. Values range from 0, indicating that all epochs were classified as low quality, to 100, indicating that all epochs were classified as high quality[36]. As in previous studies[24,61], logistic regression and group-level statistical analyses were performed with the Gini coefficient as the dependent variable to

evaluate whether ODQ, the number of participants per center, or the number of channels predicted structural inequality values.

Reporting summary

Further information on research design is available in the Nature Portfolio Reporting Summary linked to this article.

Data availability

All relevant data are included in the manuscript figures and the supplementary information. Source data underlying all graphs and charts are deposited and publicly available at Figshare, under the project name Numerical source data for graphs alpha clock EEG[104]. Row EEG files are available upon request to the Euro-LAD EEG Consortium[26]. A portion of the EEG dataset is publicly available in the BrainLat repository[27].

Code availability

The EEG processing pipeline is publicly available[81,83]. All scripts for computational analyses, including the brain age models and classifications, are released on GitHub (https://github.com/CompNeuroLabUSS/Alpha_Brain_Clocks).

Received: 8 May 2025; Accepted: 24 April 2026;
Published online: 21 May 2026

References

1. Gilbert, S. F. *Developmental Biology* (Sinauer Associates, 2000).
2. Khan, S. S., Singer, B. D. & Vaughan, D. E. Molecular and physiological manifestations and measurement of aging in humans. *Aging Cell* **16**, 624–633 (2017).
3. Cole, J. H. et al. Brain age predicts mortality. *Mol. Psychiatry* **23**, 1385–1392 (2018).
4. Gonneaud, J. et al. Accelerated functional brain aging in pre-clinical familial Alzheimer's disease. *Nat. Commun.* **12**, 5346 (2021).
5. Moguilner, S. et al. Brain clocks capture diversity and disparities in aging and dementia across geographically diverse populations. *Nat. Med.* https://doi.org/10.1038/s41591-024-03209-x (2024).
6. Bashyam, V. M. et al. MRI signatures of brain age and disease over the lifespan based on a deep brain network and 14 468 individuals worldwide. *Brain* **143**, 2312–2324 (2020).
7. Baecker, L. et al. Brain age prediction: a comparison between machine learning models using region- and voxel-based morphometric data. *Hum. Brain Mapp.* **42**, 2332–2346 (2021).
8. Chen, C.-L. et al. Generalization of diffusion magnetic resonance imaging-based brain age prediction model through transfer learning. *NeuroImage* **217**, 116831 (2020).
9. Garcia Condado, J., Cortes, J. M. & for the Alzheimer's Disease Neuroimaging Initiative NeuropsychBrainAge: a biomarker for conversion from mild cognitive impairment to Alzheimer's disease. *Alzheimer's Dement.* **15**, e12493 (2023).
10. Coronel-Oliveros, C. et al. Creative experiences and brain clocks. *Nat. Commun.* **16**, 8336 (2025).
11. Coronel-Oliveros, C. et al. Diversity-sensitive brain clocks linked to biophysical mechanisms in aging and dementia. *Nat. Mental Health* **3**, 1214–1229 (2025).
12. Millar, P. R. et al. Predicting brain age from functional connectivity in symptomatic and preclinical Alzheimer disease. *NeuroImage* **256**, 119228 (2022).
13. Engemann, D. A. et al. A reusable benchmark of brain-age prediction from M/EEG resting-state signals. *NeuroImage* **262**, 119521 (2022).
14. Engemann, D. A. et al. Combining magnetoencephalography with magnetic resonance imaging enhances learning of surrogate-biomarkers. *eLife* **9**, e54055 (2020).
15. Babiloni, C. et al. Alpha rhythm and Alzheimer's disease: has Hans Berger's dream come true? *Clinc. Neurophysiol.* **172**, 33–50 (2025).
16. Aurlien, H. et al. EEG background activity described by a large computerized database. *Clin. Neurophysiol.* **115**, 665–673 (2004).
17. Tröndle, M. et al. Decomposing age effects in EEG alpha power. *Cortex* **161**, 116–144 (2023).
18. Chu, K.-T. et al. A holo-spectral EEG analysis provides an early detection of cognitive decline and predicts the progression to Alzheimer's disease. *Front. Aging Neurosci.* **15**, 1195424 (2023).
19. Babiloni, C. et al. Sources of cortical rhythms in adults during physiological aging: a multicentric EEG study. *Hum. Brain Mapp.* **27**, 162–172 (2006).
20. Merkin, A. et al. Do age-related differences in aperiodic neural activity explain differences in resting EEG alpha? *Neurobiol. Aging* **121**, 78–87 (2023).
21. Babiloni, C. et al. Resting state cortical rhythms in mild cognitive impairment and Alzheimer's disease: electroencephalographic evidence. *JAD*. **26**, 201–214 (2011).
22. Lejko, N., Larabi, D. I., Herrmann, C. S., Aleman, A. & Ćurčić-Blake, B. Alpha power and functional connectivity in cognitive decline: a systematic review and meta-analysis. *J. Alzheimers Dis.* **78**, 1047–1088 (2020).
23. Babiloni, C. et al. Abnormalities of resting state cortical EEG rhythms in subjects with mild cognitive impairment due to Alzheimer's and Lewy body diseases. *J. Alzheimers Dis.* **62**, 247–268 (2018).
24. Hernandez, H. et al. Brain health in diverse settings: how age, demographics and cognition shape brain function. *Neuroimage* **295**, 120636 (2024).
25. Kopčanová, M. et al. Resting-state EEG signatures of Alzheimer's disease are driven by periodic but not aperiodic changes. *Neurobiol. Dis.* **190**, 106380 (2024).
26. Parra-Rodriguez, M. A. et al. The EuroLaD-EEG consortium: towards a global EEG platform for dementia, for seeking to reduce the regional impact of dementia. *Alzheimer's Dement.* **18**, e059944 (2022).
27. Prado, P. et al. The BrainLat project, a multimodal neuroimaging dataset of neurodegeneration from underrepresented backgrounds. *Sci. Data* **10**, 889 (2023).
28. Baez, S. et al. Structural inequality and temporal brain dynamics across diverse samples. *Clin. Transl. Med.* **14**, e70032 (2024).
29. Boyle, P. A. et al. The "cognitive clock": a novel indicator of brain health. *Alzheimer's Dement.* **17**, 1923–1937 (2021).
30. Klimesch, W. EEG alpha and theta oscillations reflect cognitive and memory performance: a review and analysis. *Brain Res. Brain Res. Rev.* **29**, 169–195 (1999).
31. Bazanova, O. M. & Vernon, D. Interpreting EEG alpha activity. *Neurosci. Biobehav. Rev.* **44**, 94–110 (2014).
32. Moretti, D. V. et al. Individual analysis of EEG frequency and band power in mild Alzheimer's disease. *Clin. Neurophysiol.* **115**, 299–308 (2004).
33. Babiloni, C. et al. International Federation of Clinical Neurophysiology (IFCN)—EEG research workgroup: recommendations on frequency and topographic analysis of resting state EEG rhythms. Part 1: applications in clinical research studies. *Clin. Neurophysiol.* **131**, 285–307 (2020).
34. Lundberg, S. M. & Lee, S.-I. A unified approach to interpreting model predictions. In *Advances in Neural Information Processing Systems* Vol. 30 (eds Guyon, I. et al.) (Curran Associates, Inc., 2017).
35. Gini, C. *Variabilità e Mutabilità: Contributo Allo Studio Delle Distribuzioni e Delle Relazioni Statistiche. [Fasc. I.]* (Tipografia di Paolo Cuppini, 1912).
36. Zhao, L. et al. Quantitative signal quality assessment for large-scale continuous scalp electroencephalography from a big data perspective. *Physiol. Meas.* **44**, 035009 (2023).
37. Folstein, M. F., Folstein, S. E. & McHugh, P. R. Mini-mental state". A practical method for grading the cognitive state of patients for the clinician. *J. Psychiatr. Res.* **12**, 189–198 (1975).

38. Al Zoubi, O. et al. Predicting age from brain EEG signals—a machine learning approach. *Front. Aging Neurosci.* **10**, 184 (2018).
39. Yook, S. et al. Novel neuroelectrophysiological age index associated with imaging features of brain aging and sleep disorders. *Neuroimage* **264**, 119753 (2022).
40. Kim, S. et al. Development of efficient brain age estimation method based on regional brain volume from structural magnetic resonance imaging. *Psychiatry Investig.* **21**, 37–43 (2024).
41. Xue, L. et al. 18F]FDG PET integrated with structural MRI for accurate brain age prediction. *Eur. J. Nucl. Med. Mol. Imaging* **51**, 3617–3629 (2024).
42. Yook, S., Park, H. R., Joo, E. Y. & Kim, H. Predicting the impact of CPAP on brain health: a study using the sleep EEG -derived brain age index. *Ann. Clin. Transl. Neurol.* **11**, 1172–1183 (2024).
43. Babiloni, C. et al. Resting state cortical electroencephalographic rhythms are related to gray matter volume in subjects with mild cognitive impairment and Alzheimer's disease. *Hum. Brain Mapp.* **34**, 1427–1446 (2013).
44. Babiloni, C. et al. White-matter lesions along the cholinergic tracts are related to cortical sources of EEG rhythms in amnesic mild cognitive impairment. *Hum. Brain Mapp.* **30**, 1431–1443 (2009).
45. Lopez, S. et al. The association between posterior resting-state EEG alpha rhythms and functional MRI connectivity in older adults with subjective memory complaint. *Neurobiol. Aging* **137**, 62–77 (2024).
46. Lőrincz, M. L., Kékesi, K. A., Juhász, G., Crunelli, V. & Hughes, S. W. Temporal framing of thalamic relay-mode firing by phasic inhibition during the alpha rhythm. *Neuron* **63**, 683–696 (2009).
47. Ricceri, L. et al. Cognitive and neurological deficits induced by early and prolonged basal forebrain cholinergic hypofunction in rats. *Exp. Neurol.* **189**, 162–172 (2004).
48. Babiloni, C. et al. Abnormalities of cortical neural synchronization mechanisms in subjects with mild cognitive impairment due to Alzheimer's and Parkinson's diseases: an EEG study. *J. Alzheimers Dis.* **59**, 339–358 (2017).
49. Klimesch, W., Doppelmayr, M., Russegger, H., Pachinger, T. & Schwaiger, J. Induced alpha band power changes in the human EEG and attention. *Neurosci. Lett.* **244**, 73–76 (1998).
50. Babiloni, C. et al. Resting state electroencephalographic alpha rhythms are sensitive to Alzheimer's disease mild cognitive impairment progression at a 6-month follow-up. *Neurobiol. Aging* **137**, 19–37 (2024).
51. Babiloni, C. et al. Mapping distributed sources of cortical rhythms in mild Alzheimer's disease. A multicentric EEG study. *NeuroImage* **22**, 57–67 (2004).
52. Babiloni, C. et al. Brain neural synchronization and functional coupling in Alzheimer's disease as revealed by resting state EEG rhythms. *Int. J. Psychophysiol.* **103**, 88–102 (2016).
53. Babiloni, C. et al. Occipital sources of resting-state alpha rhythms are related to local gray matter density in subjects with amnesic mild cognitive impairment and Alzheimer's disease. *Neurobiol. Aging* **36**, 556–570 (2015).
54. Moretti, D. V. et al. Volumetric differences in mapped hippocampal regions correlate with increase of high alpha rhythm in Alzheimer's disease. *Int. J. Alzheimers Dis.* **2011**, 208218 (2011).
55. Moretti, D. V., Paternicò, D., Binetti, G., Zanetti, O. & Frisoni, G. B. EEG upper/low alpha frequency power ratio relates to temporo-parietal brain atrophy and memory performances in mild cognitive impairment. *Front. Aging Neurosci.* **5**, 63 (2013).
56. Otero, M., Lea-Carnall, C., Prado, P., Escobar, M.-J. & El-Deredy, W. Modelling neural entrainment and its persistence: influence of frequency of stimulation and phase at the stimulus offset. *Biomed. Phys. Eng. Express* **8**, 045014 (2022).
57. Jones, B. F. et al. Differential regional atrophy of the cingulate gyrus in Alzheimer Disease: a volumetric MRI study. *Cereb. Cortex* **16**, 1701–1708 (2005).
58. Babiloni, C. et al. Relationship between default mode network and resting-state electroencephalographic alpha rhythms in cognitively unimpaired seniors and patients with dementia due to Alzheimer's disease. *Cereb. Cortex* **33**, 10514–10527 (2023).
59. Hafkemeijer, A. et al. Resting state functional connectivity differences between behavioral variant frontotemporal dementia and Alzheimer's disease. *Front. Hum. Neurosci*. **9**, 474 (2015).
60. Seeley, W. W. The Salience Network: a neural system for perceiving and responding to homeostatic demands. *J. Neurosci.* **39**, 9878–9882 (2019).
61. Legaz, A. et al. Structural inequality linked to brain volume and network dynamics in aging and dementia across the Americas. *Nat. Aging* **5**, 259–274 (2024).
62. Fittipaldi, S. et al. Heterogeneous factors influence social cognition across diverse settings in brain health and age-related diseases. *Nat. Mental Health* **2**, 63–75 (2024).
63. Amoruso, L. et al. Multilingualism protects against accelerated aging in cross-sectional and longitudinal analyses of 27 European countries. *Nat. Aging* **5**, 2340–2354 (2025).
64. Vidal-Pineiro, D. et al. Individual variations in 'brain age' relate to early-life factors more than to longitudinal brain change. *eLife* **10**, e69995 (2021).
65. Hammers, D. B. et al. Differences in baseline cognitive performance between participants with early-onset and late-onset Alzheimer's disease: Comparison of LEADS and ADNI. *Alzheimer's Dement.* **21**, e14218 (2025).
66. Kothe, C. A. & Makeig, S. BCILAB: a platform for brain–computer interface development. *J. Neural Eng.* **10**, 056014 (2013).
67. Delorme, A. & Makeig, S. EEGLAB: an open source toolbox for analysis of single-trial EEG dynamics including independent component analysis. *J. Neurosci. Methods* **134**, 9–21 (2004).
68. Farzan, F. et al. Standardization of electroencephalography for multi-site, multi-platform and multi-investigator studies: insights from the Canadian Biomarker Integration Network in Depression. *Sci. Rep.* **7**, 7473 (2017).
69. Bigdely-Shamlo, N. et al. Automated EEG mega-analysis II: cognitive aspects of event related features. *NeuroImage* **207**, 116054 (2020).
70. Birba, A. et al. Allostatic-interoceptive overload in frontotemporal dementia. *Biol. Psychiatry* **92**, 54–67 (2022).
71. Herzog, R. et al. Genuine high-order interactions in brain networks and neurodegeneration. *Neurobiol. Disease* **175**, 105918 (2022).
72. Cruzat, J. et al. Temporal irreversibility of large-scale brain dynamics in Alzheimer's disease. *J. Neurosci.* **43**, 1643–1656 (2023).
73. Prado, P. et al. Source space connectomics of neurodegeneration: one-metric approach does not fit all. *Neurobiol. Disease* **179**, 106047 (2023).
74. Legaz, A. et al. Social and non-social working memory in neurodegeneration. *Neurobiol. Disease* **183**, 106171 (2023).
75. Coronel-Oliveros, C. et al. Viscous dynamics associated with hypoexcitation and structural disintegration in neurodegeneration via generative whole-brain modeling. *Alzheimers Dement.* **20**, 3228–3250 (2024).
76. WorldBank. *Poverty and Inequality Platform Methodology Handbook* https://datanalytics.worldbank.org/PIP-Methodology/ (2025).
77. Creavin, S. T. et al. Mini-Mental State Examination (MMSE) for the detection of dementia in clinically unevaluated people aged 65 and over in community and primary care populations. *Cochrane Database Syst. Rev.* **2016**, CD011145 (2016).
78. Petersen, R. C. Mild cognitive impairment as a diagnostic entity. *J. Intern. Med.* **256**, 183–194 (2004).
79. McKhann, G. M. et al. The diagnosis of dementia due to Alzheimer's disease: recommendations from the National Institute on Aging-Alzheimer's Association workgroups on diagnostic guidelines for Alzheimer's disease. *Alzheimer's Dement.* **7**, 263–269 (2011).

80. Rascovsky, K. et al. Sensitivity of revised diagnostic criteria for the behavioural variant of frontotemporal dementia. *Brain* **134**, 2456–2477 (2011).
81. Prado, P. et al. Harmonized multi-metric and multi-centric assessment of EEG source space connectivity for dementia characterization. *Alzheimer's Dement.* **15**, e12455 (2023).
82. Prado, P. et al. Dementia ConnEEGtome: towards multicentric harmonization of EEG connectivity in neurodegeneration. *Int. J. Psychophysiol.* **172**, 24–38 (2022).
83. Sainz-Ballesteros, A., Perez, J. A. M., Moguilner, S., Ibáñez, A. & Prado, P. A pipeline for large-scale assessments of dementia EEG connectivity across multicentric settings. In *Methods for Analyzing Large Neuroimaging Datasets* Vol. 218 (eds Whelan, R. & Lemaître, H.) 229–253 (Springer US, 2025).
84. Dong, L. et al. MATLAB toolboxes for reference electrode standardization technique (REST) of scalp EEG. *Front. Neurosci.* **11**, 601 (2017).
85. Pion-Tonachini, L., Kreutz-Delgado, K. & Makeig, S. ICLabel: an automated electroencephalographic independent component classifier, dataset, and website. *NeuroImage* **198**, 181–197 (2019).
86. Bigdely-Shamlo, N., Kreutz-Delgado, K., Kothe, C. & Makeig, S. EyeCatch: data-mining over half a million EEG independent components to construct a fully-automated eye-component detector. *35th Annual International Conference of the IEEE Engineering in Medicine and Biology Society (EMBC)* 5845–5848 (2013).
87. Melnik, A. et al. Systems, subjects, sessions: to what extent do these factors influence EEG data? *Front. Hum. Neurosci.* **11**, 150 (2017).
88. Pascual-Marqui, R. D., Michel, C. M. & Lehmann, D. Low resolution electromagnetic tomography: a new method for localizing electrical activity in the brain. *Int. J. Psychophysiol.* **18**, 49–65 (1994).
89. Pascual-Marqui, R. D. Standardized low-resolution brain electromagnetic tomography (sLORETA): technical details. *Methods Find. Exp. Clin. Pharmacol.* **24**(Suppl. D), 5–12 (2002).
90. Rolls, E. T., Joliot, M. & Tzourio-Mazoyer, N. Implementation of a new parcellation of the orbitofrontal cortex in the automated anatomical labeling atlas. *NeuroImage* **122**, 1–5 (2015).
91. Martinez-Montes, E., Garcia-Puente, Y., Zanartu, M. & Prado-Gutierrez, P. Chirp analyzer for estimating amplitude and latency of steady-state auditory envelope following responses. *IEEE Trans. Neural Syst. Rehabil. Eng.* **28**, 2744–2753 (2020).
92. Prado-Gutierrez, P. et al. Maturational time course of the envelope following response to amplitude-modulated acoustic signals in rats. *Int. J. Audiol.* **51**, 309–316 (2012).
93. Wang, R. et al. Power spectral density and coherence analysis of Alzheimer's EEG. *Cogn. Neurodyn.* **9**, 291–304 (2015).
94. Jeong, H. T., Youn, Y. C., Sung, H.-H. & Kim, S. Y. Power spectral changes of quantitative EEG in the subjective cognitive decline: comparison of Community Normal Control Groups. *Neuropsychiatr. Dis. Treatment* **17**, 2783–2790 (2021).
95. Capilla, A. et al. The natural frequencies of the resting human brain: an MEG-based atlas. *NeuroImage* **258**, 119373 (2022).
96. Lopez, S. et al. Patients with Alzheimer's disease dementia show partially preserved parietal 'hubs' modeled from resting-state alpha electroencephalographic rhythms. *Front. Aging Neurosci.* **15**, 780014 (2023).
97. Zou, H. & Hastie, T. Regularization and variable selection via the Elastic Net. *J. R. Stat. Soc. Ser. B* **67**, 301–320 (2005).
98. James, G., Witten, D., Hastie, T. & Tibshirani, R. *An Introduction to Statistical Learning: With Applications in R* (Springer US, 2021).
99. Tian, Y. E. et al. Heterogeneous aging across multiple organ systems and prediction of chronic disease and mortality. *Nat. Med.* **29**, 1221–1231 (2023).
100. Dobbin, K. K. & Simon, R. M. Optimally splitting cases for training and testing high dimensional classifiers. *BMC Med. Genom.* **4**, 31 (2011).
101. de Lange, A.-M. G. & Cole, J. H. Commentary: Correction procedures in brain-age prediction. *Neuroimage Clin.* **26**, 102229 (2020).
102. Faul, F., Erdfelder, E., Lang, A.-G. & Buchner, A. G. Power 3: a flexible statistical power analysis program for the social, behavioral, and biomedical sciences. *Behav. Res. Methods* **39**, 175–191 (2007).
103. Moder, K. Alternatives to *F*-test in one way ANOVA in case of heterogeneity of variances (a simulation study). *Psychol. Test Assess. Model.* **52**, 343 (2010).
104. Prado, P. Numerical source data for graphs alpha clock EEG. 41661 Bytes figshare https://doi.org/10.6084/M9.FIGSHARE.31918965 (2026).

Acknowledgements

M.O. discloses support for the research of this work from Agencia Nacional de Investigación y Desarrollo (ANID) BASAL FB210008, ANID FONDECYT Iniciación 11241484 and ANID EXPLORACION 13240042. H.H. discloses support for the research of this work from the Davos Alzheimer's Collaborative (8502-2025). E.H. discloses support for the research of this work from the Interfaculty Grant of Universidad Icesi CA03130123. J.M.C. discloses support for the research of this work, Ikerbasque: The Basque Foundation for Science, and from the Spanish Ministry of Science (PID2023-148008OB-I00), Spanish Ministry of Health (PI22/01118) and Basque Ministry of Health (2025111091, 2023111002, 2022111031). M.A.P. discloses support for the research of this work from the BrainLat Seed Grant BL-SRGP2020-02. A.I. discloses support for the research of this work from the Multi-partner consortium to expand dementia research in Latin America (ReDLat2), supported by the Fogarty International Center (FIC), National Institutes of Health and National Institute on Aging (R01 AG057234, R01 AG075775, R01 AG21051, R01 AG083799, CARDS-NIH), the Alzheimer's Association (SG-20-725707), the Rainwater Charitable Foundation (The Bluefield Project to Cure FTD), ANID FONDECYT Regular (1250091, 1210176, 1220995), ANID/PIA/ANILLOS (ACT210096), JPI JPND-Care (DISCeRN 2025), ANID FONDEF (ID20I10152), ANID/FONDAP (15150012), the Wellcome Trust (335293/Z/25/Z), the Wellcome Leap CARE Program (CARE-2025-0883490149), and Horizon Europe (Marie Skłodowska-Curie Actions; CliCBrain 101236426). P.P. discloses support for the research of this work from ANID FONDECYT Regular 1260530. The contents of this publication are solely the responsibility of the authors and do not represent the official views of these institutions. The funders had no role in study design, data collection and analysis, decision to publish or preparation of the manuscript.

Author contributions

M.O., A.I, and P.P. conceived the study. A.S. and J.C. curated the data. J.C. and F.I.C. conducted the analyses. H.H and J.G.C. supervised the code implementation and data analysis. H.H., P.P., and A.I. supervised the study. M.O., A.I., and P.P. interpreted the results. M.O. wrote the first draft. P.P. designed the figures. A.I. M.O., F.I.C., C.B, A.I., and P.P. made specific contributions to sections in the manuscript. All authors reviewed, edited, provided critical comments, and approved the manuscript before submission: M.O., F.I.C., H.H., J.C., J.G.C., A.S., H.S., A.L., A.B., S.F., F.L., J.O., D.Ag., A.G., J.B., R.A.G., G.G.Y., B.G., İ.K., T.A., E.Y., L.H., R.A., P.A.V., R.G., J.E., S.L., R.W., A.F., A.M.G., D.H., M.S., E.H., D.Ab., N.R., R.A.C., W.E., J.M.C., M.A.P., C.B., A.I., and P.P.

Competing interests

The authors declare no competing interests.

Additional information

Supplementary information The online version contains supplementary material available at https://doi.org/10.1038/s42003-026-10205-z.

Correspondence and requests for materials should be addressed to Agustin Ibanez or Pavel Prado.

Peer review information *Communications Biology* thanks the anonymous reviewers for their contribution to the peer review of this work. Primary Handling Editors: Sahba Besharati and Jasmine Pan. A peer review file is available.

[1]Facultad de Ingeniería, Universidad San Sebastián, Santiago, Chile. [2]Doctorado en Biología Computacional, Universidad San Sebastián, Santiago, Chile. [3]Latin American Brain Health Institute (BrainLat), Universidad Adolfo Ibañez, Santiago, Chile. [4]Computational Neuroimaging Lab, Biobizkaia Health Research Institute, Barakaldo, Spain. [5]Pontificia Universidad Javeriana, PhD Program of Neuroscience, Bogotá, Colombia. [6]Center for Brain and Cognition, Intellectus, Bogotá, Colombia. [7]Hospital Universitario San Ignacio, Bogotá, Colombia and Universidad Nacional de Colombia, Bogotá, Colombia. [8]Cognitive Neuroscience Center, Universidad de San Andrés, Buenos Aires, Argentina. [9]School of Psychology, Trinity College Dublin, Dublin, Ireland. [10]Global Brain Health Institute (GBHI), University of California San Francisco, San Francisco, USA. [11]Global Brain Health Institute (GBHI), Trinity College Dublin, Dublin, Ireland. [12]Grupo de Neurociencias de Antioquia (GNA), University of Antioquia, Medellín, Colombia. [13]Department of Psychology, Master Program of Clinical Neuropsychology, Universidad Surcolombiana Neiva, Huila, Colombia. [14]Universidad Cooperativa de Colombia, Arauca, Colombia. [15]AG is with the Laboratorio de Neurocognición y Psicofisología, Universidad Surcolombiana, Neiva, Colombia. [16]Dokuz Eylül University, Medical School, Neurology Department, Izmir, Turkey. [17]Dokuz Eylül University, Health Sciences Institute, Neuroscience Department, Izmir, Turkey. [18]Izmir Biomedicine and Genome Center, Izmir, Turkey. [19]Department of Biophysics, School of Medicine, Istanbul Medipol University, Istanbul, Turkey. [20]Neuroscience Research Center, Research Institute for Health Sciences and Technologies, SABITA, Istanbul Medipol University, Istanbul, Turkey. [21]Dokuz Eylül University, Health Sciences Institute, Neuroscience Department, Izmir, Türkiye. [22]TA is with the Neuroscience Research Center, Research Institute for Health Sciences and Technologies (SABITA), Istanbul Medipol University, Istanbul, Turkey. [23]Section Brain Stimulation and Cognition, Department of Cognitive Neuroscience, Faculty of Psychology and Neuroscience, Maastricht University, Maastricht, The Netherlands. [24]EY is with the Istanbul Gedik University, Faculty of Health Sciences, Department of Physiotherapy and Rehabilitation, Istanbul, Turkey. [25]Istanbul Medipol University, Istanbul, Turkey. [26]Department of Neurology, Istanbul Medipol University, Istanbul, Turkey. [27]Reference Center of Behavioural Disturbances and Dementia, School of Medicine, University of Sao Paulo, Sao Paulo, Brazil. [28]Clinical Hospital of Chengdu Brain Science Institute, MOE Key Lab for Neuroinformation, University of Electronic Science and Technology of China, Chengdu, China. [29]Human Brain Mapping Department, Cuban Neuroscience Center, Habana, Cuba. [30]Institute for Imaging, Data and Communications, School of Engineering, University of Edinburgh, Edinburgh, UK. [31]Department of Physiology and Pharmacology "V. Erspamer", Sapienza University of Rome, Rome, Italy. [32]Department of Legal Medicine, Psychiatry and Pathology, Complutense University, Madrid, Spain. [33]Departamento de Lingüística y Literatura, Facultad de Humanidades, Universidad de Santiago, Santiago, Chile. [34]Center for Social and Cognitive Neuroscience (CSCN), School of Psychology, Universidad Adolfo Ibáñez, Penalolen, Santiago, Chile. [35]Universidad Católica San Pablo, Arequipa, Perú. [36]Departamento de Estudios Psicológicos, Universidad Icesi, Cali, Colombia. [37]Centre for Biomedical Engineering, School of Engineering, Faculty of Engineering and Physical Sciences, University of Surrey, Guildford, UK. [38]Institute for Complex Systems and Mathematical Biology, University of Aberdeen, Aberdeen, UK. [39]Centre for Signal and Image Processing, Department of Electronic and Electrical Engineering, University of Strathclyde, Strathclyde, UK. [40]Center of Interdisciplinary Biomedical and Engineering Research for Health, Universidad de Valparaíso, Valparaíso, Chile. [41]Department of Psychological Sciences and Health, University of Strathclyde, Glasgow, UK. [42]Hospital San Raffaele Cassino, Cassino, Italy. [43]Trinity College Dublin, The University of Dublin, Dublin, Ireland. [44]Barcelonaβeta Brain Research Center (BBRC), Pasqual Maragall Foundation, Barcelona, Spain. [45]Escuela de Fonoaudiología, Facultad de Ciencias de la Rehabilitación y Calidad de Vida, Universidad San Sebastián, Santiago, Chile. ✉e-mail: agustin.ibanez@gbhi.org; pavel.prado@uss.cl